v. 4, n. 9, 2024

Journal of
Engineering
Research

EFFECT OF WC NANOPARTICLES ON THE COBALT BASED OVERLAY DEPOSITED ON H13 STEEL BY A PLASMA TRANSFERRED ARC (PTA)

Felipe de Jesús García Vázquez
Faculty of Engineering, Autonomous University of Coahuila, Fundadores blvd. km 13 University City, ZC 35350, Arteaga, Coahuila, México.

Jesús Salvador Luna Alvarez
Faculty of Engineering, Autonomous University of Coahuila, Fundadores blvd. km 13 University City, ZC 35350, Arteaga, Coahuila, México.

J.A. Acevedo Dávila
Applied Geosciences Research Center. Autonomous University of Coahuila, Nueva Rosita 26830, Coahuila de Zaragoza México.

Gerardo Daniel Olvera Romero
Faculty of Engineering, Autonomous University of Coahuila, Fundadores blvd. km 13 University City, ZC 35350, Arteaga, Coahuila, México.

Abstract: Plasma Transferred Arc (PTA) is a process used to repair H13 steel, in which the weld deposits are characterized by low levels of inclusion and an improvement in wear resistance. In this investigation, tungsten carbide nanoparticles (WC NPs), with a size of 80 nm in average, were utilized with a nanostructure cobalt based filler metal with 0.5 and 2 wt% using sonication with ultrasonic equipment at room temperature for 30 minutes and drying at 80 °C. The nanostructured materials were analyzed using Differential Scanning Calorimetry / Thermogravimetrics (DSC/TGA) using heating and cooling rates of 20 °C/min at 1400 °C as well as being inspected by scanning electron microscopy (SEM). The filler metals were deposited by PTA on heat treated H13 steel under a 20 g/min argon flow and a 17 cm/min feed rate. Weld beads were characterized by SEM and the tribological properties were evaluated by a pin on disk test.
Keywords: Hardfacing; Tungsten carbide; H13 steel; Particle reinforced composites; PTA process.

INTRODUCTION

Hardfacing is one of the most attractive surface engineering methods employed to enhance the wear and corrosion–oxidation resistance of surfaces [1]. For this purpose the plasma transferred arc (PTA) hardfacing process is a suitable alternative compared to welding arc processes such as SMAW, GMAW and GTAW, in terms of a higher deposition rate, lower heat input, excellent arc stability and most importantly, the wide number of filler metals [2-3].

Cobalt-based alloys have had extensive use in wear related engineering applications for well over 50 years because of their inherent high-strength, corrosion resistance and ability to retain hardness at elevated temperatures [4]. Several properties of these alloys arise from the crystallographic nature of cobalt, the solid-solution-strengthening effects of chromium, tungsten and molybdenum, the formation of metal carbides, and the corrosion resistance given by chromium [5-7]. Cobalt presents a hexagonal crystal structure (hcp) at room temperature, transforming to a cubic form (fcc) at higher temperatures (above 400 °C). The stacking fault energy of both allotropes is low, which offers better response to stress [7]. Chromium also provides oxidation and corrosion resistance by forming an adherent oxide film at high temperatures while refractory metals such as molybdenum and tungsten contribute to strength via precipitation hardening by forming MC and M_6C carbides and intermetallic phases such as Co_3 (Mo, W) [8].

Stellite alloys are a group of cobalt-based superalloys with the main constituents belonging to the quaternary systems Co–Cr–W–C or Co–Cr–Mo–C. These alloys are generally strengthened by the precipitation of carbides in their cobalt matrix. The most important differences among Stellite alloys are their carbon and tungsten contents, which affect the type and amount of carbide formation in their microstructures [9]. The aim of this work is to study the effect of WC NPs on the microstructure, hardness and abrasive sliding wear behavior in cobalt-based Stellite 12 deposited overlays. This alloy was nanostructured with 0.5 and 2 wt% WC NPs and deposited by Plasma Transferred Arc (PTA) on heat treated hot work tool steel.

EXPERIMENTAL PROCEDURE

PREPARATION OF NANOSTRUCTURED FILLER METAL

For the impregnation of the Stellite 12 filler metal (150/45 μm, Kennametal) with WC NPs (80 nm, Skyspring Nanomaterials), the WC NPs were dispersed in 250 ml of ethanol and sonicated for 1 h separately. Subsequently, the

filler metal was placed into the dispersed WC NPs and sonicated for 3 h. This sonication process promotes the incorporation of WC NPs into the secondary interdendritic branches of the filler metals. This process was carried out with 0.5 and 2 wt% of WC NPs in the Stellite 12 filler metal, respectively. These samples are labeled as Stellite 12 without NPs (ST1), Stellite 12 with 0.5 and 2wt% of WC NPs (ST2) and (ST3), respectively.

THERMAL EVOLUTION OF FILLER METAL WITH AND WITHOUT WC NANOPARTICLES

The reactivity of WC NPs on the Stellite 12 filler metal was determined by thermal evolution of each sample in a sealed tube furnace under an Ar gas flow of 10 mL/min at 1400 °C in a TA Instruments model 660 using heating/cooling rates of 20 °C/min. The maximum heating temperature (1400°C) was selected in terms of the melting range established in the technical data of Stellite 12 (1200-1365 °C).

ALLOY DEPOSITION AND WELD METAL CHARACTERIZATION

Hot work tool steel plates (H13) were thermally treated before the welding process. This thermal treatment was carried out by preheating at 845 °C for 1 h followed by an austenizing at 1020 °C for 45 min and quenching in circulating air. After that, the samples were tempered twice at 595 °C for 2 h in order to reach a microhardness of 499 HV in order to have the best microstructural condition. The Stellite 12 with and without WC NPs were deposited on 25 mm thick AISI H13 heat-treated hot work tool steel, using the PTA overlaying process shown in Figure 1. The PTA equipment consists of two power sources, one the Fronius Transtig 1700 to the pilot arc and the Fronius Transtig 4000 to the plasma arc. The parameters used in this study are listed in Table 1. The metal powders injected from a powder feeder are melted inside the plasma arc flame and the melted metal powders thus obtained are deposited on the substrate.

The coated samples were polished mechanically and chemically etched by submerging them in a solution of H_3PO_4(10%) + H_2SO_4(50%) + HNO_3(40%) in order to reveal their microstructures. These samples were examined at high amplifications using a Nikon SMZ745T stereo, a Nikon Eclipse MA200 optical and a JEOL JSM-6490LV model scanning electron microscope (SEM) fitted with an Oxford Instruments INCA x-sight model energy dispersive X-ray analyzer (EDS). The microhardness of the samples was measured in Vickers across the overlay, the heat affected zone and the unaffected substrate with a Wilson Tukon 2500 automated Knoop / Vickers microhardness tester, with a load of 0.5 kg (HV0.5).

MEASUREMENTS OF MICROHARDNESS AND WEAR RESISTANCE ON THE OVERLAY.

The tribological behavior of overlays was investigated under sliding wear using a CSM pin-on-disk tribometer, as per ASTM: G99-05. During the test, the specimen was spinning at a linear speed of 10 cm/s over a distance of 1000 m. The pin was placed at a distance of 6 mm from the rotation center on the specimen surface under a compressive force of 5N without lubrication. As a result of friction/ wear, a circular wear track was created on the specimen surface. The pin was a sapphire ball of 6 mm in diameter. The loss due to wear was evaluated by calculating the volume of the wear track after the specimen surface was worn for 2.78 h. The friction was recorded automatically throughout the test with the aid of a linear variable displacement transducer and the coefficient of friction was calculated

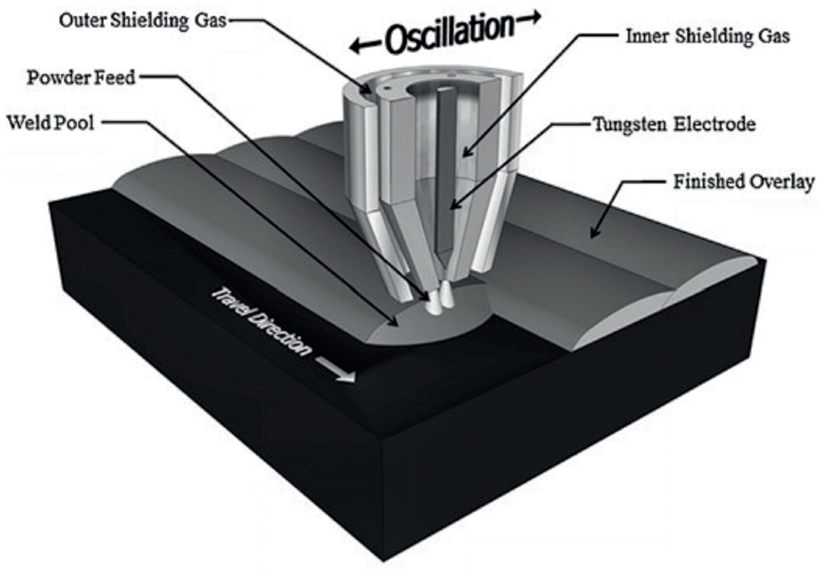

Figure 1. Schematics of the PTA process used for depositing wear resistant overlays [10]

Parameters	
Main arc current (A)	165
Travel speed rate (cm/min)	17
Powder feed rate (g/min)	20
Torch gap (mm)	10
Shielding gas - Ar (lpm)	12
Plasma gas - Ar (lpm)	5
Carrier gas - Ar (lpm)	5
Preheating (°C)	350

Table 1. PTA welding parameters

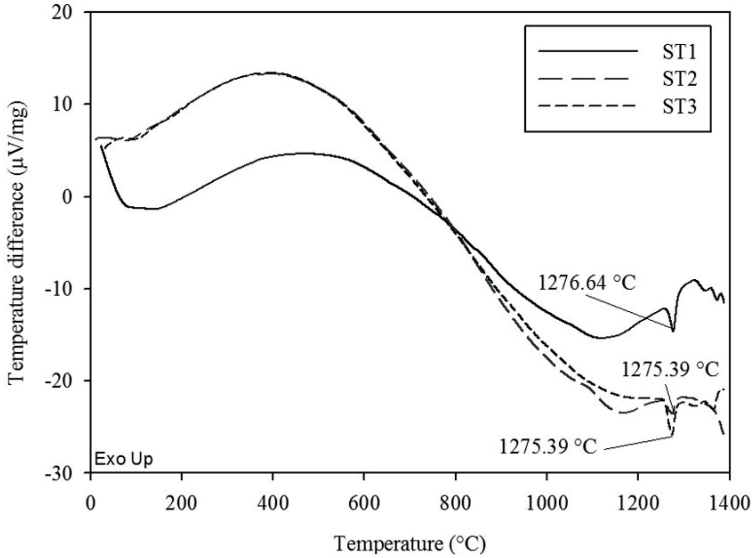

Figure 2. DSC curves of Stellite 12 without WC NPs (ST1) and with 0.5 and 2 wt% of WC NPs (ST2) and (ST3), respectively.

in real time with the built-in software.

RESULTS AND DISCUSSION

THERMAL ANALYSIS OF FILLER METAL WITH AND WITHOUT WC NANOPARTICLES

Figure 2 illustrates the heating cycle of the DSC test and presents the phase transformation curves. Generally, differential thermal analysis conducted on the samples with and without WC NPs in the temperature range between 1100 and 1280°C manifested endothermic events. With an increase in the content of 2 wt% of WC NPs, the first endothermic event of ST3 is displaced at 1275.39 °C. By contrast, ST1 and ST2 have only a slight displacement. On the other hand, the following endothermic events in samples ST1, ST2 and ST3 suggest that a liquid/solid phase sintering be adopted. The maximum sintering temperature should be selected around the peak temperature of the first transformation phase [11], which is 1276.64 °C for ST1, 1275.39 °C for ST2 and 1275.39 °C for ST3. Likewise, the eutectic phases of Stellite cannot be changed by the addition of WC NPs due to the fact that these samples have endothermic events at the same temperatures. This involves an increase in the heat adsorption of the sample while the addition of WC NPs is raised, which results in more energy needed per mass unit to perform the phase transformation.

ALLOY DEPOSITION AND WELD METAL CHARACTERIZATION

The chemical composition of H13 steel substrate and filler metal with and without WC NPs is presented in Table 2. A characteristic of the steel substrate is the contents of C, Mo, Cr, Nb and V, which influence in the precipitation of strengthening carbides that increase the mechanical properties at high temperatures. In the case of filler metals, the Co improves corrosion resistance and ability to retain hardness at high temperatures and precipitate as Co_3Ti, a phase coherent with the matrix. In addition, reports in literature [12-14] suggest that the cooling of the PTA deposited Stellite 12 overlay from the liquid state involves a primary Co-rich solid solution dendritic matrix and the remaining liquid eventually solidifies by means of a eutectic reaction into a lamellar mixture of a Co-rich solid solution phase with Cr-rich carbides [15]. The W and C in WC for ST2 and ST3 can act as reinforcing particulars in the overlays by forming rings for dislocations with the particles as has been presented in the work of Orowan [16], given as:

$$\tau_o = \frac{Gb}{\lambda} \quad (1)$$

where τ_o is shear stress (MPa); G is shear module (GPa); b is Burgers vector (nm) and λ is interparticle spacing (nm).

Figure 3 shows, at high amplifications, the microstructures of the cross-section of the examined overlays of ST1, ST2 and ST3, respectively. As can be appreciated, the overlays have a dendritic microstructure with phases dispersed among the interdendritic regions in the cobalt-rich matrix. Because of that, an enriched liquid fraction of eutectic is trapped during the solidification. The literature suggests that a lamellar eutectic mixture of an fcc phase and M_7C_3 eutectic carbides is formed because of a eutectic reaction in an inter-dendritic region of the remaining liquid [17].

Comparatively, the Stellite 12 impregnated with WC NPs allows a slight refinement of the microstructure thereby giving rise to the reduction of the inter-dendritic region as shown in Figure3 (b) and (c). It is postulated that the WC NPs can increase the rate of nucleation into the metallic pool rather than dendritic growth. In this case, the solidification is started with a greater content

Material	Co	Cr	W	C	Ni	Mo	Fe	Si	Mn	P	Cu	V	WC NPs
AISI H13	-	4.15	0.051	0.37	0.11	1.31	Bal.	1.18	0.29	0.026	0.072	0.948	-
ST1	Bal.	30	8.5	1.45	2	0.9	1	1	-	-	-	-	-
ST2	Bal.	29.85	8.46	1.44	1.99	0.9	1	1	-	-	-	-	0.5
ST3	Bal.	29.4	8.33	1.42	1.96	0.88	0.98	0.98	-	-	-	-	2

Table 2. Chemical composition (wt%) of hot work tool steel substrate, pure filler metal and combinations with WC NPs

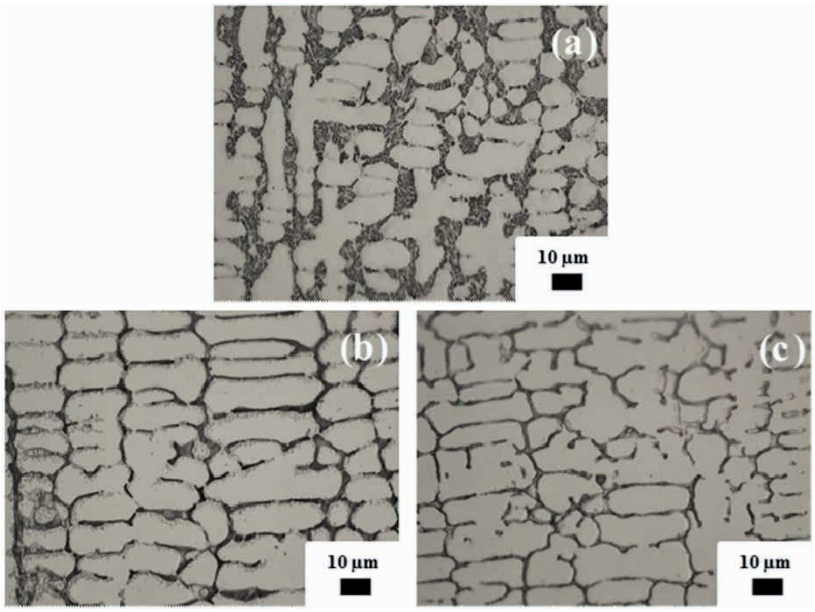

Figure 3. Optical micrograph 1000X of the microstructure of (a) ST1, (b) ST2 and (c) ST3

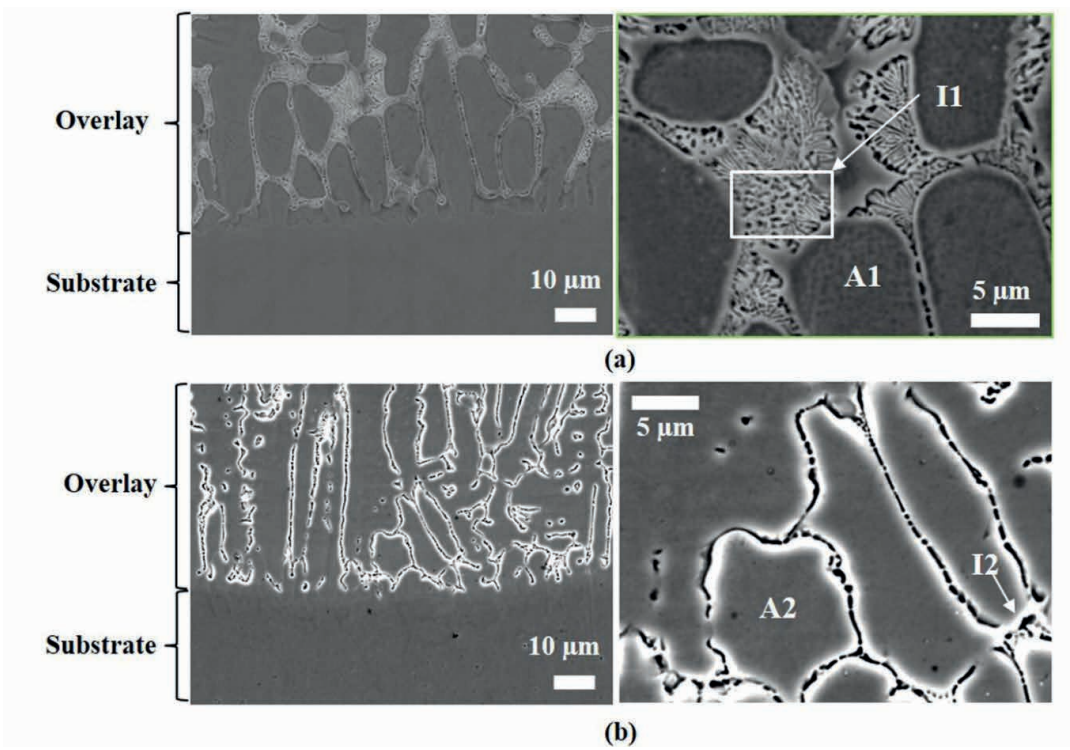

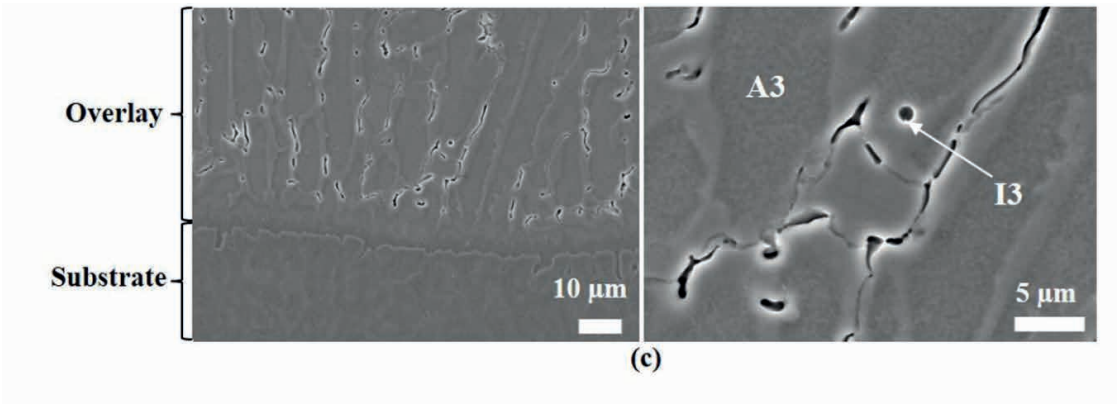

Figure 4. SEM images of (a) overlay/substrate interface of ST1 without WC NPs, (b) ST2 with WC NPs at 0.5 wt% and (c) ST3 WC NPs at 2 wt%

	A1	A2	A3	I1	I2	I3
C	23.86	27.67	29.35	17.58	11.56	22.93
Si	1.77	1.81	1.51	-	2.2	1.11
S	-	0.3	0.36	0.71	0.8	0.6
Cr	14.66	11.07	8.98	17.38	12.52	11.6
Mn	0.36	0.36	-	0.48	0.42	0.36
Fe	32.35	42.06	47.83	32.5	51.57	51.32
Co	26.09	16.05	11.32	29.1	19.53	11.48
W	0.91	0.67	0.65	2.26	1.4	0.59

Table 3. EDS analysis (wt%) of the constituents present in the microstructures of the examined

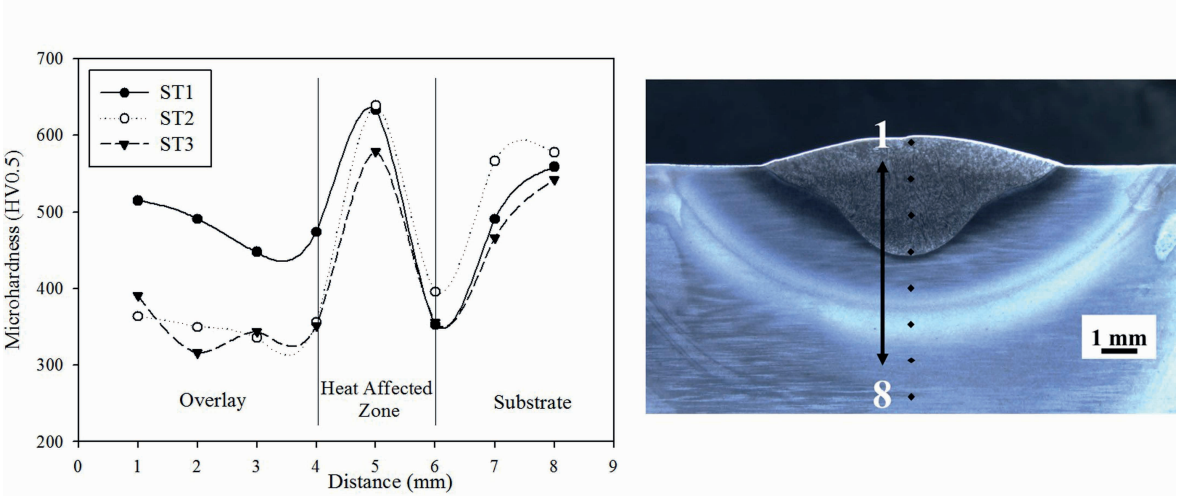

Figure 5. Microhardness profile (left) and microhardness indentations across the sample (right)

of solid fraction in the samples with WC NPs.

Figure 4 (a) shows a demarcated area with interdendritic regions and lamellar eutectic phases (I1). Moreover, Figure 4 shows a good metallurgical bonding between the substrate and overlays after solidification of the metallic pool with and without 0.5 and 2 wt% of WC NPs. This fact is due to the high thermal gradient and analogous chemical nature, which leads to the high diffusing effect in the interface of filler metal and substrate [18]. In Figure 4 (b) carbides in the boundary of dendritic were observed (I2) as well as spherical morphology (I3) (Figure 4 (c)).

Table 3 summarizes the elemental chemical composition of the overlays using EDX analysis. The dendritic matrix (A1 region) of the unmodified Stellite 12 overlay (ST1) mainly consisted of carbon, chromium, iron and cobalt with a small amount of silicon, manganese and tungsten. It is noticeable that the addition of WC NPs (ST2 and ST3) to the original alloy (ST1) reduced the interdendritic zone, and the main constituents of dendritic matrix (A2 and A3 region) were modified, i.e. an increase in carbon and iron wt% and a decrease in chromium, cobalt and tungsten wt% were reached. A similar behavior was observed in the interdendritic zone, where the lamellar eutectic, (Fig. 4 (a), I1 region) rich on carbon, chromium, iron and cobalt wt%, was modified with the addition of WC NPs resulted in a globular shape, a reduction of the interdendritic zone (I2 and I3 region, Table 3), an increase in carbon and iron wt%, and a decrease in chromium, cobalt and tungsten wt%. EDX analysis conducted on ST1, ST2 and ST3 revealed that the iron diffused from the substrate to the overlay, while WC NPs were added, according to the atomic percentages observed in Table 3.

MEASUREMENTS OF MICROHARDNESS AND WEAR RESISTANCE OF THE OVERLAY

Overall, it is accepted that the microhardness of a material is related closely to its resistance to wear [9, 19]. In order to correlate the microhardness with wear resistance and compare the effect of WC NPs on the overlay, in this work, 10 indentations (Figure 5 (b)) were made along three regions (overlay, HAZ and substrate) in samples ST1, ST2 and ST3, and then the pin-on-disk test was carried out with a 5 N load.

The microhardness behavior analyzed through the three regions in each sample (ST1, ST2 and ST3) is similar. However, the impregnation of WC NPs in the cobalt-based Stellite 12 alloy reduced the microhardness of the overlay (Fig. 5 (a)). These microhardness results are directly related to the effect on the inter-dendritic spacing. This result is consistent with the information analyzed that shows the reduction of the carbide formation that consequently reduced the overlay microhardness.

Wear test results are presented as volume loss in Figure 6. The weight loss was converted to volume loss using material density, and then was normalized by the load and sliding distance. It is shown that the best weight loss result was obtained in ST2, followed by ST1 and ST3 respectively. In this graph the effect of WC NPs is remarkable, showing an increase in wear resistance. But when the addition of WC NPs is increased to 2 wt%, wear resistance decreases, which results in greater volume loss. The wear rate showed the same behavior as the volume loss, where ST2 exhibited the highest wear resistance with a low wear rate of about 4.5×10^{-6} mm^3/Nm with a 5N load.

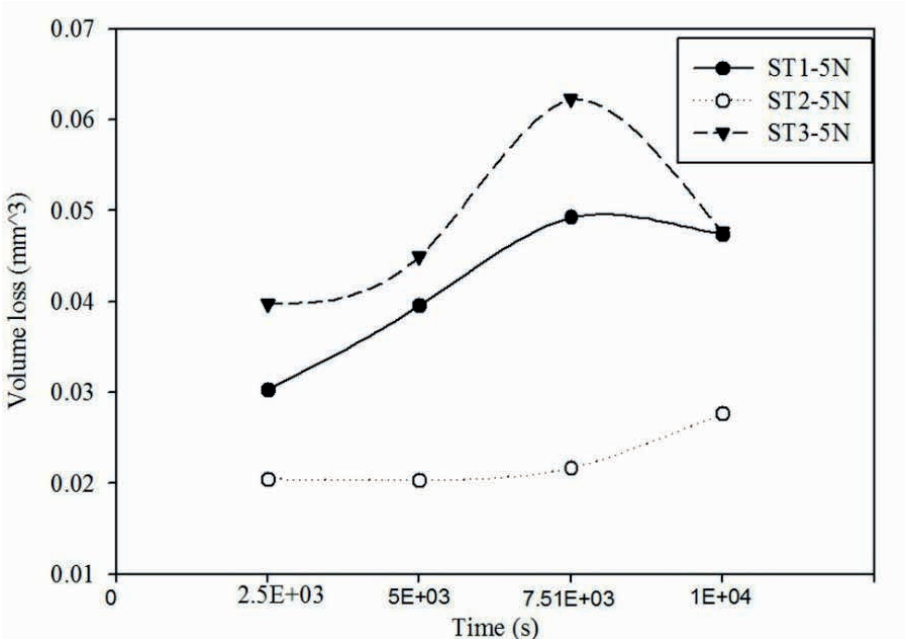

Figure 6. Pin on disk wear test results, volume loss at 5 N load

CONCLUSIONS

Within the framework of the experimental conditions used here, it was found that the addition of WC NPs to Stellite 12 do not affect the melting point, but that the rate of heat flow is faster in the Stellite 12 without WC NPs that in the others samples with WC NPs. It is a postulate that the melting point of WC NPs is higher than the sintering temperature of Stellite 12 at which WC NPs are still stable, as shown in the DSC curves. This phenomenon requires further study.

The interdendritic regions are modified and refined by the incorporation of WC NPs. It is remarkable that, in the presence of an increase in the weight percentage of WC NPs, the interdendritic regions are reduced. Due to that, the solidification starts with a major liquid fraction in major nucleation sites.

The interdendritic regions contain a higher content of lamellar eutectic phases than the samples without WC NPs. Likewise, all samples with and without WC NPs have good metallurgical bonding between the substrate and overlay.

Wear resistance is better in the sample with 0.5 wt% of WC NPs than in the samples with a higher content of nanoparticles. It can be postulated that small precipitates are dissolved into a metallic pool. In consequence, these solidified precipitates in the matrix can interact with dislocations that are generated by friction, thus increasing wear resistance. As well, these samples contain a minor interdendritic region without eutectic phases. Currently, the authors are working with other techniques in order to elucidate the role of the precipitates after wear testing and to propose a correlation between the sizes of precipitates and wear, so as to, to propose an alternative route to increase wear and corrosion resistance by the incorporation of WC NPs (wt%).

REFERENCES

[1] ANTONY, K.; BHANSALI, K.; MESSLER, R.; MILLER, A.; PRICE, M. Hardfacing. ASM Handbook, vol.6, p.771-780, 1983.

[2] CHEN, D.; LIU, D.; LIU, Y.; WANG, H.; HUANG, Z. Microstructure and fretting wear resistance of γ/TiC composite coating in situ fabricated by plasma transferred arc cladding, Surface and Coatings Technology, vol.239, p.28-33, 2014. DOI: 10.1016/j.surfcoat.2013.11.012.

[3] SHIN, J.C.; DOH, J.M.; YOON, J.K.; LEE, D.Y.; KIM, J.S. Effect of molybdenum on the microstructure and wear resistance of cobalt-base Stellite hardfacing alloys, Surface and Coatings Technology, vol.166(2), p.117-126, 2003. DOI 10.1016/S0257-8972(02)00853-8.

[4] NEVILLE, A.; HODGKIESS, T. Characterization of high-grade alloy behavior in severe erosion–corrosion conditions, Wear, vol.233, p.596-607, 1999. DOI 10.1016/S0043-1648(99)00220-3.

[5] CROOK, P. Properties and Selection: Nonferrous Alloys and Special-Purpose Materials, Metals Handbook, 10. ed., vol.2, p.446, 1993.

[6] DAVIS, J. R. Nickel, cobalt, and their alloys, ASM international, 2000.

[7] BETTERIDGE, W. Cobalt and its alloys, Chichester: Halsted Press, 1982.

[8] BIROL, Y. Thermal fatigue testing of Stellite 6-coated hot work tool steel, Materials Science and Engineering: A, vol.527(21), p.6091-6097, 2010. DOI 10.1016/j.msea.2010.06.015.

[9] KHODDAMZADEH, A.; LIU, R.; LIANG, M.; YANG, Q. Wear resistant carbon fiber reinforced Stellite alloy composites, Materials & Design, vol.56, p.487-494, 2014. DOI 10.1016/j.matdes.2013.11.034.

[10] MENDEZ, P.F.; BARNES, N.; BELL, K.; BORLE, S.D. Welding processes for wear resistant overlays, Journal of Manufacturing Processes, vol.16(1), p.4-25, 2014. DOI 10.1016/j.jmapro.2013.06.011.

[11] OPRIS, C.D.; LIU, R. Development of Stellite alloy composites with sintering/HIPing technique for wear-resistant applications, Materials & design, vol.28(2), p.581-591, 2007. DOI 10.1016/j.matdes.2005.08.004.

[12] HUANG, P.; LIU, R.; WU, X.; YAO, M.X. Effects of molybdenum content and heat treatment on mechanical and tribological properties of a low-carbon Stellite alloy, Journal of Engineering Materials and Technology, vol.129(4), p.523-529, 2007. DOI 10.1115/1.2744429.

[13] WOOD, P.D.; EVANS, H.E. Investigation into the wear behaviour of Stellite 6 during rotation as an unlubricated bearing at 600 °C, Tribology International, vol.44(12), p.1589-1597, 2011. DOI 10.1016/j. triboint.2011.02.011.

[14] YU, H.; AHMED, R.; VILLIERS LOVELOCK, H. A comparison of the tribo-mechanical properties of a wear resistant cobalt-based alloy produced by different manufacturing processes, Journal of tribology, vol.129(3), p.586-594, 2007. DOI 10.1115/1.2736450.

[15] MOTALLEBZADEH, A.; ATAR, E.; CIMENOGLU, H. Sliding wear characteristics of molybdenum containing Stellite 12 coating at elevated temperatures, Tribology International, vol.91, p.40-47, 2015. DOI 10.1016/j.triboint.2015.06.006.

[16] DIETER, G.E.; BACON, D.J. Mechanical metallurgy, vol.3, New York: McGraw-Hill, 1986.

[17] ATAMERT, S.; BHADESHIA, H.K. Comparison of the microstructures and abrasive wear properties of Stellite hardfacing alloys deposited by arc welding and laser cladding, Metallurgical Transactions A, vol.20(6), p.1037-1054, 1989. DOI 10.1007/BF02650140.

[18] HOU, Q.Y.; GAO, J.S.; ZHOU, F. Microstructure and wear characteristics of cobalt-based alloy deposited by plasma transferred arc weld surfacing, Surface and Coatings Technology, vol.194(2), p.238-243, 2005. DOI 10.1016/j.surfcoat.2004.07.065.

[19] KONYASHIN, I.; RIES, B.; ZHUK, Y.; MAZILKIN, A.; STRAUMAL, B.; PARK, D. Wear resistance and hardness: Are they directly related for nanostructured hard materials?, International Journal of Refractory Metals and Hard Materials, vol.49, p.203-211, 2015. DOI 10.1016/j.ijrmhm.2014.06.017.